INSTITUTE OF PHYSICS PUBLISHING JOURNAL OF NEURAL ENGINEERING

J. Neural Eng. **3** (2006) 1–8 doi:10.1088/1741-2560/3/1/001

Role of electrode design on the volume of tissue activated during deep brain stimulation

Christopher R Butson and Cameron C McIntyre

Department of Biomedical Engineering, Cleveland Clinic Foundation, Cleveland, OH, USA

E-mail: mcintyc@ccf.org

Received 12 August 2005
Accepted for publication 7 November 2005
Published 19 December 2005
Online at stacks.iop.org/JNE/3/1

Abstract

Deep brain stimulation (DBS) is an established clinical treatment for a range of neurological disorders. Depending on the disease state of the patient, different anatomical structures such as the ventral intermediate nucleus of the thalamus (VIM), the subthalamic nucleus or the globus pallidus are targeted for stimulation. However, the same electrode design is currently used in nearly all DBS applications, even though substantial morphological and anatomical differences exist between the various target nuclei. The fundamental goal of this study was to develop a theoretical understanding of the impact of changes in the DBS electrode contact geometry on the volume of tissue activated (VTA) during stimulation. Finite element models of the electrodes and surrounding medium were coupled to cable models of myelinated axons to predict the VTA as a function of stimulation parameter settings and electrode design. Clinical DBS electrodes have cylindrical contacts 1.27 mm in diameter (d) and 1.5 mm in height (h). Our results show that changes in contact height and diameter can substantially modulate the size and shape of the VTA, even when contact surface area is preserved. Electrode designs with a low aspect ratio (d/h) maximize the VTA by providing greater spread of the stimulation parallel to the electrode shaft without sacrificing lateral spread. The results of this study provide the foundation necessary to customize electrode design and VTA shape for specific anatomical targets, and an example is presented for the VIM. A range of opportunities exist to engineer DBS systems to maximize stimulation of the target area while minimizing stimulation of non-target areas. Therefore, it may be possible to improve therapeutic benefit and minimize side effects from DBS with the design of target-specific electrodes.

Introduction

Deep brain stimulation (DBS) is an established therapy for essential tremor (Benabid *et al* 1996), Parkinson's disease (Obeso *et al* 2001) and dystonia (Vidailhet *et al* 2005). In addition, DBS shows promise in the treatment of other disorders such as epilepsy (Hodaie *et al* 2002), obsessive–compulsive disorder (Gabriels *et al* 2003) and depression (Mayberg *et al* 2005). However, the current clinical DBS electrode design was adapted from cardiac pacing technology ~20 years ago without knowledge of several fundamental neurostimulation principles that have only recently been elucidated. In addition, advances in computational capabilities and neural engineering design tools that couple finite element method (FEM) electric field models with multi-compartment neuron models have provided the ability to quantitatively evaluate the neural response to DBS in a controlled environment (McIntyre *et al* 2004b, 2004c, Butson *et al* 2005a, Butson and McIntyre 2005). In turn, a unique opportunity exists to design theoretically optimal DBS electrodes, customized to the anatomy and morphology of the stimulation target, with the goal of improving the therapeutic benefits of the device.

One of the first steps toward customizing DBS electrodes for different anatomical targets and/or disease states is characterization of the electric field and volume of tissue activated (VTA) by stimulation. The electric field is dependent on the electrode contact geometry, the distribution

of cathode(s) and anode(s) and the biophysical properties of the tissue medium (Malmivuo and Plonsey 1995). The neural response to the electric field is related to the second spatial derivative (activating function) of the extracellular potentials generated along each neural process (McNeal 1976, Rattay 1986, Warman *et al* 1992).

The primary goal of this study was to apply detailed computer modeling techniques to the quantitative evaluation of a range of DBS electrode designs. To achieve this goal, we first developed a new method to predict the VTA as a function of stimulation parameters and electrode design. Traditionally, the technique of coupling electric field data to multi-compartment neuron models (field-neuron models) has been used to predict the neural response to extracellular stimulation (McNeal 1976). However, the use of field-neuron models is computationally intensive, limits the applicability of the results to the explicit electrode and neuron geometries studied, and requires a large number of simulations to define a 3D surface representative of the VTA. Alternatively, activating function-based approaches provide a general measure of neural activation directly from the electric field data and consequently have several computational advantages over the field-neuron approach (Rattay 1986, Warman *et al* 1992). However, previous attempts to characterize the activating function for prediction of neural activation have shown significant errors in this technique (Warman *et al* 1992, Zierhofer 2001, Moffitt *et al* 2004). Therefore, we augmented this general approach with a new method to improve the accuracy of threshold prediction. With this new technique, we performed a quantitative comparison of the VTAs generated by a range of clinically relevant DBS electrode geometries and stimulation parameter settings. We hypothesize that it is possible to control the shape and extent of the VTA through careful control of electrode geometry. We demonstrate this concept by customizing an electrode design for a specific anatomical target, the ventral intermediate nucleus (VIM) of the thalamus, a common surgical target for the treatment of tremor (Benabid *et al* 1996).

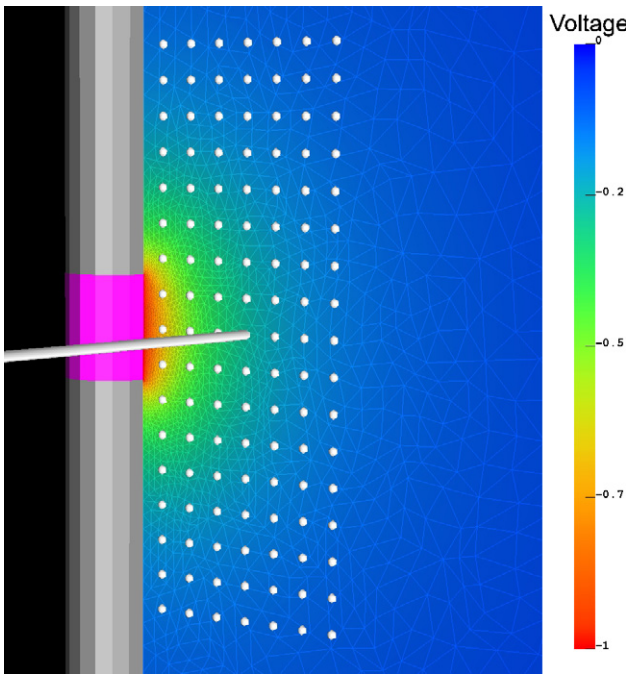

Figure 1. Field-axon model. Axisymmetric FEM (wireframe) of the electrode (shaft: gray, contact: pink) and surrounding medium ($\sigma = 0.3$ S m^{-1}) with voltage solution according to colorbar at right. The 17 × 7 array of axons was oriented perpendicular to the electrode shaft as shown for a single representative fiber (white spheres indicate positions of other axons). The voltage solution was interpolated onto the cable model axons for calculation of the stimulus voltage thresholds and $\Delta^2 V_e/\Delta x^2$ threshold values.

Methods

The goals of this study were to develop quantitative techniques to predict the VTA as a function of arbitrary stimulation parameters and electrode geometry, and to use those techniques to customize the electrode design to a target nucleus. Converging theoretical (McIntyre *et al* 2004b) and experimental (Hashimoto *et al* 2003) results suggest that DBS generates an excitatory effect on axons surrounding the electrode. While correlations between axonal activation and the therapeutic mechanisms of DBS remain controversial, one leading hypothesis is that high frequency stimulation results in an override of the underlying pathological neural activity patterns (Montgomery and Baker 2000, Hashimoto *et al* 2003, Grill *et al* 2004, McIntyre *et al* 2004a). Therefore, we concentrated our analysis on the characterization of axonal activation with DBS.

Neural stimulation was estimated with an integrated model that combined FEM electric field solutions with multi-compartment cable models of myelinated axons. The electric field generated during monopolar stimulation by the DBS electrode was calculated from the Poisson equation with a Fourier FEM solver to determine time- and space-dependent voltage within the tissue medium (Butson and McIntyre 2005). The voltage waveforms were subsequently interpolated onto cable model axons distributed around the electrode, and threshold values of the stimulation voltage necessary for action potential generation were calculated. The second spatial difference of the extracellular potential distribution ($\Delta^2 V_e/\Delta x^2$) at the site of action potential initiation was determined at the stimulation threshold for each axon ($\Delta x =$ internodal spacing of 0.5 mm). The $\Delta^2 V_e/\Delta x^2$ solutions were used to create a VTA prediction scheme as a function of stimulation parameters.

Finite element model

Axisymmetric FEM models of DBS electrodes with approximately 13 000 nodes were constructed in FEMLAB v3.1 (Comsol Inc, Burlington, MA) (figure 1) as previously described (Butson and McIntyre 2005). The tissue medium was modeled as homogeneous and isotropic with conductivity $\sigma = 0.3$ S m^{-1}. The axisymmetric volume conductor measured 100 mm tall by 50 mm wide. Electrode contact dimensions ranged from 0.25 mm to 2.5 mm in diameter and from 0.5 mm to 3.8 mm in height. These dimensions were centered around

the Medtronic 3387/3389 quadripolar DBS electrode contact dimensions (1.5 mm height, 1.27 mm diameter) (Medtronic Inc, Minneapolis, MN). The electrode lead was modeled as an electrical insulator with the exception of the contact area, which was used for voltage-controlled stimulation. Stimulation voltage was specified at the contact surface, and the Poisson equation was solved for the voltage within the tissue medium using the Fourier FEM solver (Butson and McIntyre 2005). While the Poisson equation alone provides a spatial voltage solution, it does not account for the time dependence of the stimulus waveform or the capacitance of the electrode–tissue interface. The Fourier FEM solver overcomes these limitations by using a complex stiffness matrix that represents the capacitance of the electrode–tissue interface, and by solving the Poisson equation at multiple frequencies to reconstruct the time-dependent stimulus waveform. The resulting solutions are both time- and space-dependent, and incorporate the effects of electrode capacitance on the stimulus waveform delivered to the tissue during voltage-controlled stimulation (Butson and McIntyre 2005).

Neural stimulation prediction

Field-axon simulations were conducted using Fourier FEM DBS electrode models coupled to 5.7 μm diameter myelinated axon models (McIntyre *et al* 2002, Butson and McIntyre 2005). A collection of 119 model axons were distributed in a 17 $\times$ 7 matrix oriented perpendicular to the electrode shaft (figure 1). This orientation of axons was used to identify the spatial extent of activation in the vertical and horizontal directions relative to the electrode shaft (localization of activation in axons oriented parallel to the shaft would be ambiguous in the vertical direction). The axons were placed 1 mm to 4 mm lateral to the electrode and +4 mm above to -4 mm below the center of the electrode contact. Each model axon included 21 nodes of Ranvier with 0.5 mm internodal spacing.

The time-dependent potential distribution generated in the tissue medium from the Fourier FEM solution was interpolated onto the length of each axon, and the time-dependent transmembrane potential variations induced by the stimulation were calculated in NEURON v5.7 (Hines and Carnevale 1997). Threshold stimulus amplitudes were defined that generated action potentials in a one-to-one ratio with a stimulus frequency of 130 Hz, representative of typical clinical DBS parameter settings (Volkmann *et al* 2002). The threshold values were used to create 2D contours to define the boundary of activation as a function of the stimulus amplitude. These contours were swept around the axis of the electrode to determine the VTA.

An alternative approach to the computationally intensive field-neuron simulations described above is the use of an activating function-based technique (Rattay 1986). The second difference of the extracellular potential distribution along a neural process ($\Delta^2V_e/\Delta x^2$) provides a quantitative estimate of the polarization of the neuron in response to an applied electric field. One attractive feature of this method is that for a given stimulus pulse width, $\Delta^2V_e/\Delta x^2$ threshold values are relatively constant across a wide range of electrode designs (see the results section, figure 3(A)). However, $\Delta^2V_e/\Delta x^2$ alone is not an accurate predictor of neural activation (Warman *et al* 1992, Zierhofer 2001, Moffitt *et al* 2004). As a first approximation, a $\Delta^2V_e/\Delta x^2$ threshold value can be selected and the spread of stimulation can be defined by the volume of tissue encompassed by that criteria. However, this overestimates activation near the electrode and underestimates activation distant to the electrode. An alternative is to create a $\Delta^2V_e/\Delta x^2$ threshold curve fit as a function of electrode to axon distance (figure 2(A)). This technique has the advantage of providing accurate threshold values across all electrode–axon distances, but a separate curve must be generated for each pulse width. Further, this method fails to accommodate different electrode designs and breaks down for electrodes with a small diameter/height aspect ratio (figure 2(B)).

A third approach that addresses the limitations mentioned above is to determine $\Delta^2V_e/\Delta x^2$ threshold values as a function of pulse width and voltage. Specifically, $\Delta^2V_e/\Delta x^2$ threshold values are recorded, and these values are expressed as a function of cathodic voltage (V) times pulse width (PW, μs) (figure 2(C)). This expression allows two stimulation parameters to be condensed into a single number for prediction of thresholds. Further, threshold values recorded this way were found to be valid for a wide range of electrode designs and stimulation parameters. These values can then be used to create 2D spatial contours that are swept around the z-axis to define the VTA volume (figure 2(D)). For purposes of volume calculations, it is often convenient to describe the VTA contours with analytical functions. To do so, each contour is described by an ellipse:

$$(x - x_0)^2/a^2 + (y - y_0)^2/b^2 = 1$$

where x_0, y_0 is the center of the ellipse, and a and b are the semimajor and semiminor axes, respectively (assuming $b < a$). The semimajor and semiminor coefficients are calculated from the following: a = distance of threshold value from electrode contact along x-axis; b = maximum y value of 2D threshold contour. Under the model conditions used in this study, the electrode contact is centered on the origin and the center of each ellipse is $x_0 = a$, $y_0 = 0$. With this method, $\Delta^2V_e/\Delta x^2$ threshold values and VTA volumes can be predicted for a wide range of electrode designs and stimulation parameters.

In this study, we solved the complete field-axon model for each electrode design shown in figure 3 to build the $\Delta^2V_e/\Delta x^2$ threshold relationships. Our motivation for this exercise was twofold. First, we wanted to provide analytical functions that could be used by other DBS investigators, who may not have the expertise to develop full field-axon models, thereby allowing relatively accurate predictions for their own studies. Second, we believe that generalized $\Delta^2V_e/\Delta x^2$ threshold relationships, developed under idealized conditions, can be useful for rapid evaluation of a given electrode design and/or stimulation parameter settings in a more complicated environment. For example, we have recently

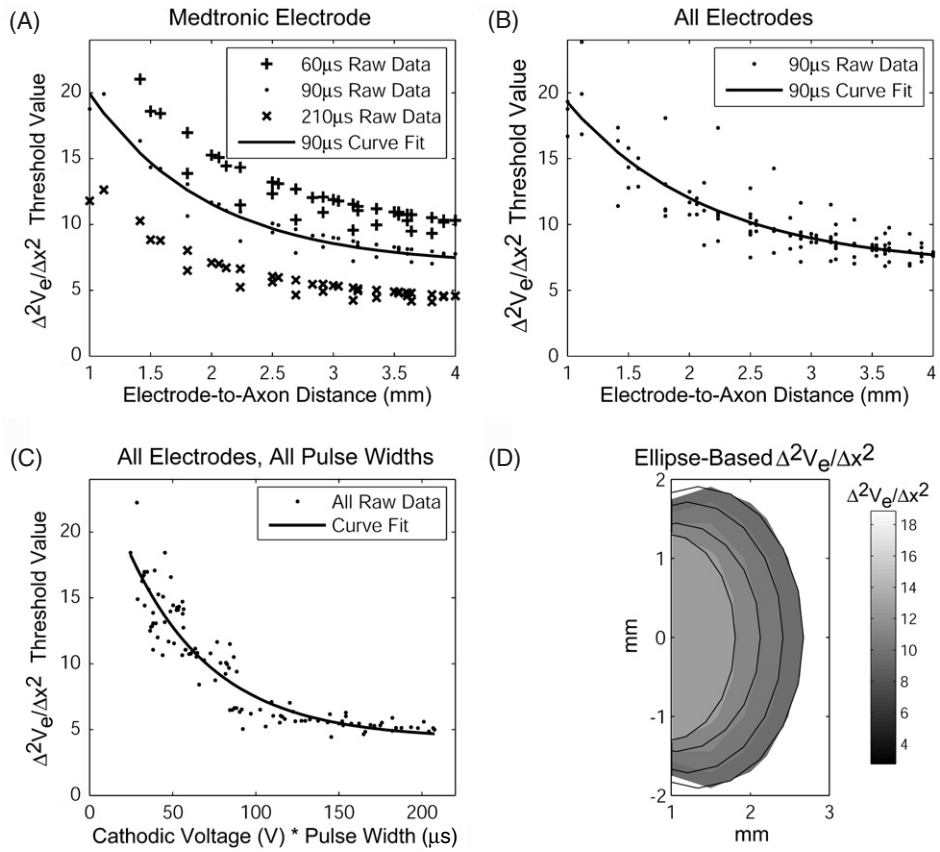

Figure 2. $\Delta^2 V_e/\Delta x^2$ as a predictor of neural activation. (A) $\Delta^2 V_e/\Delta x^2$ threshold values are shown for the Medtronic electrode as a function of distance measured from the center of the electrode for 60 μs, 90 μs and 210 μs pulse width. An exponential curve fit (solid line shown for 90 μs, $y = 36.38\,e^{-x/.97} + 6.89$) can provide accurate prediction of activating function thresholds for individual pulse widths and electrode designs. (B) However, the predictor curve used in part (A) does not extend well to multiple electrode designs. Here, raw data are shown for all electrode designs used in figure 3(A) for 90 μs pulse width; the accuracy of the curve fit ($y = 29.88\,e^{-x/1.14} + 6.80$) is limited by the increased variability of threshold values. (C) A more general predictor that is applicable to the range of electrode designs and pulse widths expresses the activating function as a function of cathodic voltage (V) $*$ pulse width (PW, μs) (curve fit: $y = 22.70\,e^{-x/50.90} + 4.30$). Raw data are shown for the three electrode designs from figure 3(A) for 60 μs, 90 μs and 210 μs pulse width stimulation. (D) Ellipsoid-based predictors (black lines) can provide a spatial map of activation for a variety of electrode designs and stimulation parameters. In this example, the ellipse predictors for voltage-controlled stimulation are overlaid on filled $\Delta^2 V_e/\Delta x^2$ threshold contours (color bar at right) generated from the integrated field-axon model for 90 μs pulse width.

developed DBS models derived from human diffusion tensor magnetic resonance imaging data that can be customized to individual patients (Butson *et al* 2004, 2005b, McIntyre *et al* 2004c). However, the prospect of running full field-axon simulations to make VTA predictions for pre-operative electrode targeting or post-operative stimulation parameter selection is highly unrealistic given the thousands of permutations that may be necessary to find an optimal electrode location and/or stimulation parameter setting. Our $\Delta^2 V_e/\Delta x^2$ threshold relationships provide a computationally efficient VTA prediction technique to apply DBS modeling to clinical research. Further, we have used our $\Delta^2 V_e/\Delta x^2$ threshold relationships in this study to evaluate the VTA generated by electrode contacts designs with heights and diameters that fall between electrode geometries for which we have full field-axon data (figures 3 and 4). In turn, we are able to more quickly and efficiently search the parameter space for electrode design optimization applications.

Results

Effects of electrode geometry on the VTA

We examined the effects of electrode geometry on the VTA by co-varying the height and radius of the electrode contact to maintain a constant surface area. In all cases, the results were evaluated relative to the Medtronic 3387/3389 electrode contact dimensions (1.27 mm diameter, 1.5 mm height, 5.98 mm^2 surface area) under a range of clinically relevant stimulation parameters (figure 3). Stimulus voltage and pulse width modulated the VTA for each electrode design (figure 3(A)). The VTA aspect ratio, determined by dividing VTA diameter/height, was identified as a useful metric to quantify VTA shape and was correlated with electrode dimensions (figure 3(B)). Increases in electrode contact height caused a linear increase in VTA volume; the rate of increase was dependent on the stimulation pulse width (figure 3(C)). Increases in electrode contact diameter caused a logarithmic

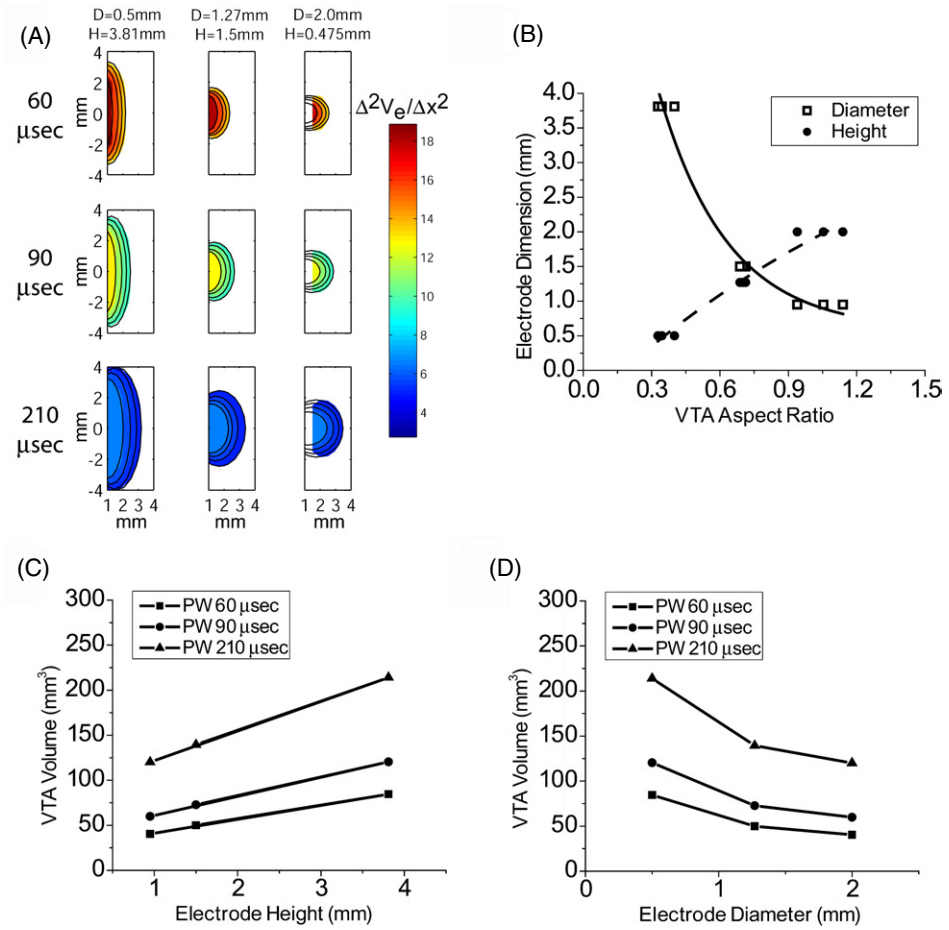

Figure 3. Effects of electrode geometry on VTA for constant surface area electrodes. (A) Filled contour plots show $\Delta^2 V_e/\Delta x^2$ threshold values corresponding to the colorbar at right. Each plot shows the VTA at four voltage values (−0.4 V, −0.6 V, −0.8 V, and −1.0 V) for 130 Hz stimulation. Plots are organized by pulse width (rows) and electrode design (columns). (B) Electrode diameter and height are correlated with VTA aspect ratio. Data are shown for all pulse widths at a stimulus amplitude of −1 V. (C) VTA volume increases linearly with electrode height. The slope of each line is modulated by pulse width. (D) VTA volume decreases in a roughly logarithmic fashion with increasing diameter, modulated by pulse width.

decrease in VTA volume, also proportional to the stimulation pulse width (figure 3(D)). Since contacts with the same surface area have roughly the same average current density for a given set of stimulation parameters, these simulations demonstrate that the VTA shape and volume can be modulated by changing electrode geometry alone.

Customized electrode design for thalamic stimulation

The VIM of thalamus represents a common surgical target for DBS control of tremor (Benabid *et al* 1996). However, anatomical definition of the VIM cannot be accurately defined on traditional magnetic resonance images. In turn, brain atlases are commonly used to estimate the size and shape of the VIM. We used a 3D surface rendering of the thalamus and VIM from the T1 MRI of a normal human brain, previously developed using a software created by Surgical Navigation Technologies (personal communication, Henderson J M) (figure 4(A)). The resulting volumes of the thalamus and VIM for this brain were 4365 mm^3 and 218 mm^3, respectively. The VIM is a long, narrow nucleus measuring ∼8 mm (dorsal–ventral) by ∼3 mm (anterior–posterior) by ∼12 mm (medial–lateral) (figure 4(B)). While the VTA produced by the Medtronic DBS electrode design encompasses part of the VIM, it is not possible to generate a good match between the shape of the nucleus and the VTA. The aspect ratio of the Medtronic VTA was ∼0.7 with a volume of 57 mm^3 using stimulation parameters of −1 V, 90 μs and 130 Hz, with only 26% of the VIM activated by the VTA (figure 4(C)). The VIM would be better suited to a long, narrow VTA that matched the aspect ratio of the nucleus. The desired VTA aspect ratio would be ∼3 mm (anterior–posterior diameter)/∼8 mm (dorsal–ventral height) ≈ 0.4. Given manufacturing limitations of the lead tubing which must accommodate four coiled conductor wires and the insertion stylet, the traditional DBS leads are limited to a minimum diameter of ∼0.75 mm. A contact height of 2.54 mm and diameter of 0.75 mm result in a VTA aspect ratio of nearly 0.4, better matching the dimensions of the VIM and maintaining contact surface area for safe stimulation limits. This customized electrode design for VIM generated a VTA of 73 mm^3 with a −1 V, 90 μs, 130 Hz stimulus train, and a 28% increase compared to the current clinical DBS

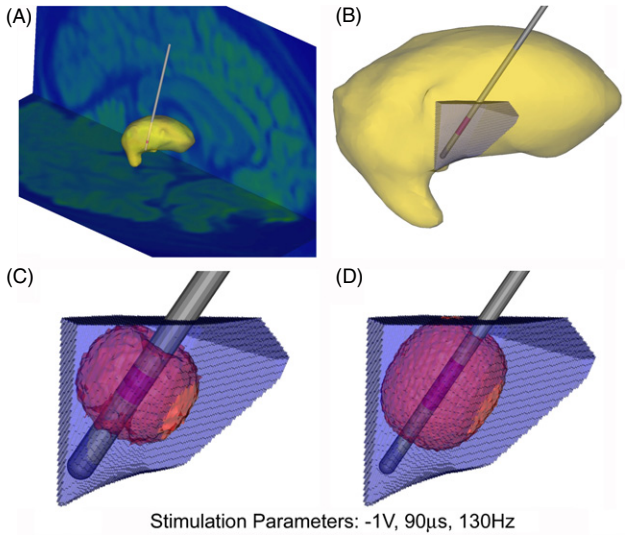

Figure 4. Thalamic VIM stimulation with different electrode designs. (A) 3D view of thalamus with DBS electrode and T1 MRI projected onto background slices. (B) VIM within thalamus with a DBS electrode. (C) The Medtronic electrode, with stimulation settings of -1 V and 90 μs pulse width, produces a VTA that fills 26% of the VIM before spilling over into adjacent nuclei. (D) The VIM is better stimulated using an electrode with 0.75 mm diameter and 2.54 mm height, producing a VTA that fills 33% of the volume without spillover.

electrode design. In addition, the customized electrode design stimulated 7% more of the VIM with no increase in spread to neighboring structures (figure 4(D)).

Discussion

The fundamental goal of this study was to perform a quantitative evaluation of a range of DBS electrode designs. Our intentions were to define specific characteristics of the VTA size and shape that correlate with the size and shape of the stimulating electrode contact. This theoretical understanding of the interaction between the electrode geometry and the stimulated tissue provides two important considerations for the future design of DBS electrodes. First, our results suggest that it is possible to maximize the efficacy of the charge delivered to the tissue by maximizing the VTA for a given electrode surface area. Second, we show that the size and shape of the VTA can be changed by manipulating electrode geometry, thereby opening the door for customization of the electrode design to the anatomical and morphological properties of the surgical target.

Study limitations

The results of this study provide a quantitative analysis on the impact of changes in DBS electrode design on the volume of tissue activated by stimulation. However, the results probably represent an overestimation of the VTA for a variety of reasons. First, the myelinated axon model used for stimulation prediction was of relatively large diameter (5.7 μm) for the central nervous system. Large diameter myelinated axons represent the most excitable neural elements surrounding extracellular stimulating electrodes (Ranck 1975, McIntyre and Grill 2000). A more realistic mix of fiber sizes and neuron types would provide more detailed information on the overall neural response to DBS. Second, all nodes of Ranvier along the fibers were in plane with the electrode (i.e. at the closest possible point to the electrode contact), facilitating inward current flow and maximal depolarization. A more random alignment of nodes of Ranvier relative to the electrode contact may also reduce the VTA. Third, the electric field model did not take into account the low conductivity encapsulation layer that surrounds the electrode *in vivo*. Encapsulation limits the spread of current around the electrode and can reduce the VTA by up to 50% (Butson *et al* 2005a). An additional limitation was our use of a homogeneous and isotropic tissue medium, rather than biophysically based conductivities. We have previously developed models of DBS that incorporate inhomogeneous and anisotropic tissue conductivities derived from diffusion tensor magnetic resonance imaging data (Butson *et al* 2004, McIntyre *et al* 2004c). However, for the purposes of this study we chose to concentrate on the impact of electrode design on the electric field in the most controlled environment possible. In future studies, we will address these limitations, with the goal of accurately predicting VTAs under more realistic clinical conditions. In the interim, the data presented in this study should be interpreted as a worst-case scenario of VTA spread as a function of electrode design and the stimulation parameters.

DBS electrode design customized to the surgical target

The original design of the Medtronic 3387/3389 electrode contact was hindered by limited knowledge of the neural stimulation objectives of the device. Recent advances in neural engineering design tools, such as the computer modeling techniques used in this study, were not available when DBS was invented. In addition, the therapeutic mechanisms of action remain an issue of controversy (McIntyre *et al* 2004a). Until direct neurophysiological relationships can be determined between the stimulation and therapeutic benefit, true engineering optimization of DBS electrode design will remain difficult. However, the results of this study show that modified electrode designs can be used to customize the VTA to specific target nuclei.

The behavioral effects induced by DBS depend on the exact location of the stimulation electrode, the choice of stimulation parameters and the type/position/orientation of the various neural elements subjected to the stimulation. Our simplified approach of defining the VTA with a single neuron type and orientation and using that VTA as a guide for electrode design clearly fails to capture many important issues that could impact the efficacy of the device. However, we believe our techniques represent an improvement over previous trial-and-error strategies.

To demonstrate the concept of DBS electrode customization to a surgical target, we designed an electrode for the VIM of thalamus (figure 4). There is a considerable debate in the DBS literature on methods for locating the VIM, the optimal site of stimulation within the nucleus and whether

therapeutic benefit is better correlated with stimulation spread to adjacent structures (Caparros-Lefebvre *et al* 1999, Mobin *et al* 1999, Dowsey-Limousin 2002, Garonzik *et al* 2002, Krack *et al* 2002, Gross *et al* 2004). The purpose of this study was not to strictly define the target volume for VIM stimulation but rather to demonstrate how electrodes can be customized to stimulate a given volume in a clinically relevant context.

This study concentrated on DBS electrode design in the context of monopolar stimulation. However, existing (and future) DBS electrodes enable the selection of multiple stimulating contacts as either anodes or cathodes to provide additional flexibility in shaping the VTA. For example, selection of two adjacent electrode contacts (1.5 mm gap for the Medtronic 3387 electrode) as cathodes will generate a cumulative VTA with a relatively small aspect ratio. Interestingly, clinicians have identified this phenomenon empirically in the context of stimulation parameter selection for VIM DBS where it is not uncommon to find therapeutic stimulation parameter settings with multiple adjacent cathodes (Dowsey-Limousin 2002). In turn, significant engineering design opportunities exist to improve not only the individual electrode contacts, but also the number and spacing the contacts on the electrode shaft. For example, it may be beneficial to have a relatively large contact, with a VTA aspect ratio optimized for a given anatomical target, flanked by smaller tightly spaced contacts above and below the optimal contact to provide additional control of dorsal/ventral stimulation spread. Advances in our understanding of the neural response to high frequency stimulation, coupled to better definition of the therapeutic target volume of tissue to be stimulated within the various DBS surgical targets, will allow ever-improving theoretical design of these medical devices.

Acknowledgments

This work was supported by grants from the American Parkinson Disease Association, the Ohio Biomedical Research and Technology Transfer Partnership and the National Institutes of Health (NS-50449 & NS-52042). The authors would also like to thank Jaimie Henderson for the thalamic reconstructions, John Hall for technical assistance and Ali Rezai for conceptual assistance.

References

Benabid A L, Pollak P, Gao D, Hoffmann D, Limousin P, Gay E, Payen I and Benazzouz A 1996 Chronic electrical stimulation of the ventralis intermedius nucleus of the thalamus as a treatment of movement disorders *J. Neurosurg.* **84** 203–14

Butson C R, Hall J, Henderson J M and McIntyre C C 2004 Patient-specific models of deep brain stimulation: 3D visualization of anatomy, electrode and volume of activation as a function of the stimulation parameters *Soc. Neurosci. Abstr.* 1011.11

Butson C R, Maks C B, Cooper S E, Henderson J M and McIntyre C C 2005b Deep brain stimulation interactive visualization system *Soc. Neurosci. Abstr.* 898.7

Butson C R, Maks C B and McIntyre C C 2005a Sources and effects of electrode impedance during deep brain stimulation *Clin. Neurophysiol.* at press

Butson C R and McIntyre C C 2005 Tissue and electrode capacitance reduce neural activation volumes during deep brain stimulation *Clin. Neurophysiol.* **116** 2490–500

Caparros-Lefebvre D, Blond S, Feltin M P, Pollak P and Benabid A L 1999 Improvement of levodopa induced dyskinesias by thalamic deep brain stimulation is related to slight variation in electrode placement: possible involvement of the centre median and parafascicularis complex *J. Neurol. Neurosurg. Psychiatry* **67** 308–14

Dowsey-Limousin P 2002 Postoperative management of Vim DBS for tremor *Mov. Disord.* (Suppl. 3) **17** S208–11

Gabriels L, Cosyns P, Nuttin B, Demeulemeester H and Gybels J 2003 Deep brain stimulation for treatment-refractory obsessive-compulsive disorder: psychopathological and neuropsychological outcome in three cases *Acta Psychiatr. Scand.* **107** 275–82

Garonzik I M, Hua S E, Ohara S and Lenz F A 2002 Intraoperative microelectrode and semi-microelectrode recording during the physiological localization of the thalamic nucleus ventral intermediate *Mov. Disord.* (Suppl. 3) **17** S135–44

Grill W M, Snyder A N and Miocinovic S 2004 Deep brain stimulation creates an informational lesion of the stimulated nucleus *Neuroreport* **15** 1137–40

Gross R E, Jones E G, Dostrovsky J O, Bergeron C, Lang A E and Lozano A M 2004 Histological analysis of the location of effective thalamic stimulation for tremor. Case report *J. Neurosurg.* **100** 547–52

Hashimoto T, Elder C M, Okun M S, Patrick S K and Vitek J L 2003 Stimulation of the subthalamic nucleus changes the firing pattern of pallidal neurons *J. Neurosci.* **23** 1916–23

Hines M L and Carnevale N T 1997 The NEURON simulation environment *Neural Comput.* **9** 1179–209

Hodaie M, Wennberg R A, Dostrovsky J O and Lozano A M 2002 Chronic anterior thalamus stimulation for intractable epilepsy *Epilepsia* **43** 603–8

Krack P, Dostrovsky J, Ilinsky I, Kultas-Ilinsky K, Lenz F, Lozano A and Vitek J 2002 Surgery of the motor thalamus: problems with the present nomenclatures *Mov. Disord.* (Suppl. 3) **17** S2–8

Malmivuo J and Plonsey R 1995 *Bioelectromagnetism: Principles and Applications of Bioelectric and Biomagnetic Fields* (New York: Oxford University Press)

Mayberg H S, Lozano A M, Voon V, McNeely H E, Seminowicz D, Hamani C, Schwalb J M and Kennedy S H 2005 Deep brain stimulation for treatment-resistant depression *Neuron* **45** 651–60

McIntyre C C and Grill W M 2000 Selective microstimulation of central nervous system neurons *Ann. Biomed. Eng.* **28** 219–33

McIntyre C C, Grill W M, Sherman D L and Thakor N V 2004b Cellular effects of deep brain stimulation: model-based analysis of activation and inhibition *J. Neurophysiol.* **91** 1457–69

McIntyre C C, Mori S, Sherman D L, Thakor N V and Vitek J L 2004c Electric field and stimulating influence generated by deep brain stimulation of the subthalamic nucleus *Clin. Neurophysiol.* **115** 589–95

McIntyre C C, Richardson A G and Grill W M 2002 Modeling the excitability of mammalian nerve fibers: influence of afterpotentials on the recovery cycle *J. Neurophysiol.* **87** 995–1006

McIntyre C C, Savasta M, Kerkerian-Le Goff L and Vitek J L 2004a Uncovering the mechanism (s) of action of deep brain stimulation: activation, inhibition, or both *Clin. Neurophysiol.* **115** 1239–48

McNeal D R 1976 Analysis of a model for excitation of myelinated nerve *IEEE Trans. Biomed. Eng.* **23** 329–37

Mobin F, De Salles A A, Behnke E J and Frysinger R 1999 Correlation between MRI-based stereotactic thalamic deep brain stimulation electrode placement, macroelectrode

stimulation and clinical response to tremor control *Stereotact. Funct. Neurosurg.* **72** 225–32
Moffitt M A, McIntyre C C and Grill W M 2004 Prediction of myelinated nerve fiber stimulation thresholds: limitations of linear models *IEEE Trans. Biomed. Eng.* **51** 229–36
Montgomery E B Jr and Baker K B 2000 Mechanisms of deep brain stimulation and future technical developments *Neurol. Res.* **22** 259–66
Obeso J A, Olanow C W, Rodriguez-Oroz M C, Krack P, Kumar R and Lang A E 2001 Deep-brain stimulation of the subthalamic nucleus or the pars interna of the globus pallidus in Parkinson's disease *N. Engl. J. Med.* **345** 956–63
Ranck J B 1975 Which elements are excited in electrical stimulation of mammalian central nervous system: a review *Brain Res.* **98** 417–40
Rattay F 1986 Analysis of models for external stimulation of axons *IEEE Trans. Biomed. Eng.* **33** 974–77
Vidailhet M *et al* 2005 Bilateral deep-brain stimulation of the globus pallidus in primary generalized dystonia *N. Engl. J. Med.* **352** 459–67
Volkmann J, Herzog J, Kopper F and Deuschl G 2002 Introduction to the programming of deep brain stimulators *Mov. Disord.* **17** S181–7
Warman E N, Grill W M and Durand D 1992 Modeling the effects of electric fields on nerve fibers: determination of excitation thresholds *IEEE Trans. Biomed. Eng.* **39** 1244–54
Zierhofer C M 2001 Analysis of a linear model for electrical stimulation of axons—critical remarks on the 'activating function concept' *IEEE Trans. Biomed. Eng.* **48** 173–84